

# APEX: Action Priors Enable Efficient Exploration for Skill Imitation on Articulated Robots

Shivam Sood\*, Laukik B Nakhwa\*, Yuhong Cao, Sun Ge, Guillaume Sartoretti

Department of Mechanical Engineering, National University of Singapore, Singapore  
 shivamsood@nus.edu.sg, laukiknakhwa@gmail.com, caoyuhong@nus.edu.sg,  
 sunge@nus.edu.sg, guillaume.sartoretti@nus.edu.sg

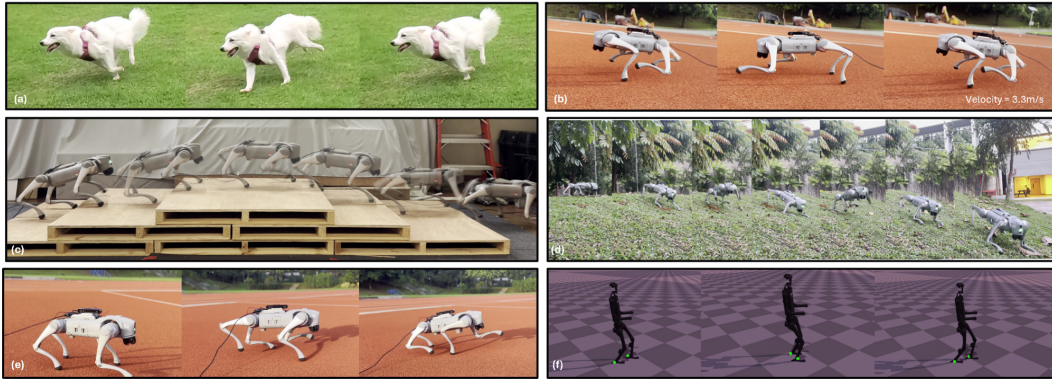


Figure 1: (a) A Japanese Spitz exhibiting a canter (b) Learned canter gait using animal motion capture data achieves peak speeds  $> 3.3\text{m/s}$  (c,d) Generalization to stairs and slopes using only flat-ground imitation data preserving the gait trot and canter respectively (e) Gait adaptation based on velocity using a single reinforcement learning policy (f) Extension of APEX to humanoids.

**Abstract:** Learning by imitation provides an effective way for robots to develop well-regulated complex behaviors and directly benefit from natural demonstrations. State-of-the-art imitation learning (IL) approaches typically leverage Adversarial Motion Priors (AMP), which, despite their impressive results, suffer from two key limitations. They are prone to mode collapse, which often leads to overfitting to the simulation environment and thus increased sim-to-real gap, and they struggle to learn diverse behaviors effectively. To overcome these limitations, we introduce **APEX** (Action Priors enable Efficient Exploration): a simple yet versatile imitation learning framework that integrates demonstrations directly into reinforcement learning (RL), maintaining high exploration while grounding behavior with expert-informed priors. We achieve this through a combination of decaying action priors, which initially bias exploration toward expert demonstrations but gradually allow the policy to explore independently. This is complemented by a multi-critic RL framework that effectively balances stylistic consistency with task performance. Our approach achieves sample-efficient imitation learning and enables the acquisition of diverse skills within a single policy. APEX generalizes to varying velocities and preserves reference-like styles across complex tasks such as navigating rough terrain and climbing stairs, utilizing only flat-terrain kinematic motion data as a prior. We validate our framework through extensive hardware experiments on the Unitree Go2 quadruped. There, APEX yields diverse and agile locomotion gaits, inherent gait transitions, and the highest reported speed for the platform to the best of our knowledge ( $\sim 4.5\text{m/s}$  in sim-to-sim transfer, and a peak velocity of  $\sim 3.3\text{m/s}$  on hardware). Our results establish APEX as a compelling alternative to existing IL methods, offering better efficiency, adaptability, and real-world performance. Video link: <https://youtu.be/f6GKpPCyOGY>

**Keywords:** Imitation Learning, Locomotion, Reinforcement Learning

# 1 Introduction

Legged robots hold the promise of replicating the agility, robustness, and adaptability showcased by their animal counterparts. These capabilities are critical for real-world deployments in complex scenarios such as disaster response [1], where robots must recover from perturbations and traverse unstructured terrain by smoothly transitioning among gaits. This requires overcoming significant control challenges due to the underactuated and highly dynamic nature of legged locomotion.

Traditional approaches to legged locomotion have primarily relied on optimal control techniques, often leveraging predefined gaits optimized for specific tasks [2, 3, 4, 5, 6]. While effective for structured environments, these methods struggle to generalize to unseen tasks and can be computationally expensive. To address these limitations, the community has widely turned to Reinforcement Learning (RL), which can leverage the full dynamics of the robot, generalize better to unseen tasks, and enable compute-efficient deployment on hardware [7, 8, 9, 10, 11]. However, learning-based methods remain notoriously hard to train. They demand careful reward engineering and often extensive curriculum design, including progressive environment difficulty, adaptive termination conditions, and adaptive domain randomization to balance policy exploration and exploitation.

Imitation learning (IL), which leverages expert demonstrations, provides a promising way of addressing these issues. Supervised IL approaches like Behavioral Cloning (BC) [12] offer simple and efficient learning but often struggle with generalization due to distributional shift, i.e., recovering from mistakes not in the dataset. In contrast, adversarial imitation learning (IL) methods [13] have become central to many recent state-of-the-art approaches [14, 15, 16]. At their core, these methods employ a GAN-style discriminator to distinguish between expert demonstrations and agent-generated behavior, using this feedback to guide policy learning. This framework has enabled substantial progress in both robotic and character-level imitation learning. However, they suffer from well-known limitations, the main one being *mode collapse*, i.e., overfitting to simulation environments, which increases the sim-to-real gap [17, 18] and hampers real-world deployment. Furthermore, these methods often struggle to capture diverse behaviors within a single policy and can be sample inefficient, requiring long training times. Recent works typically rely on models training latent variables, separate policies for individual motions, and/or high-level controllers to sequence them [17, 15, 19]. On the other hand, diffusion-based imitation learning methods excel at modeling diverse behaviors [17], but their high computational cost, action latency, and multi-step denoising hinder real-time control and limit deployment in dynamic real-world settings.

To address the key challenges, we propose APEX, a combined RL and IL algorithm that emphasizes exploration over just supervision. We develop this expert-guided RL framework by leveraging *action priors* [20] as “scaffolds” during training, which can help guide the agent’s exploration without restraining it. Unlike prior approaches, we do not rely on GANs or diffusion models, thereby avoiding mode collapse and enabling more stable training and improved sim-to-real transfer. We provide theoretical and empirical evidence demonstrating how blended policy optimization with action priors can improve exploration efficiency while remaining anchored to expert data. Furthermore, we show that our multi-critic network structure and scaffolded exploration can work synergistically to allow the agent to explore beyond mere imitation, adapting to environments not covered by demonstration data. Finally, we integrate reference-state initialization (RSI) and phase-based tracking into APEX, enabling the learning of diverse and smoothly transitioning skills within a single policy, even though such transitions were never present in the imitation dataset.

We validate the effectiveness of APEX through extensive simulation and hardware experiments on the Unitree Go2 quadruped, demonstrating its ability to learn different gaits and smooth transitions among them, adapt these gaits to novel environments, and achieve the highest reported velocity in the literature to the best of our knowledge. We also benchmark APEX against AMP across multiple gaits, showing how APEX requires only kinematic data, whereas AMP and other motion imitation frameworks [21, 22, 11] typically need full-state information, including joint and body velocities. We finally present preliminary results on humanoid locomotion, illustrating that APEX generalizes beyond quadrupeds to other robotic platforms. We believe that these results establish APEX as a new practical and scalable approach to imitation learning for legged robotics.

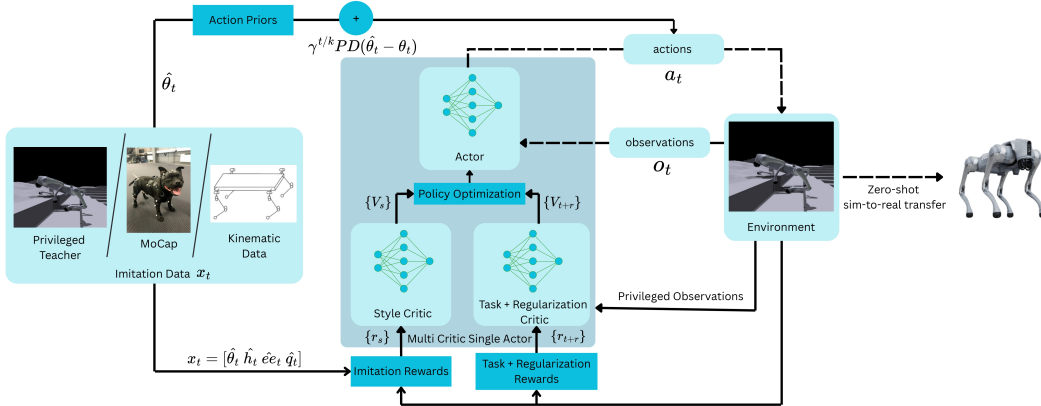


Figure 2: Overview of APEX. Only dashed lines are required during deployment; 1) **Imitation data** can be collected from either a privileged teacher policy, motion capture data or other sources like animation; 2) **Action Priors** (sec 2.1) are the feed-forward torques calculated from collected kinematic joint data and added to the actions to bias exploration; 3) **Multi-critic RL** (sec 2.2) PPO algorithm is used to train the final motion with both style and task+regularization rewards; 4) the trained policy is transferred to the hardware zero-shot.

## 2 APEX Framework for Expert-Guided Imitation Learning

First, we show how action priors bias exploration toward the style of the demonstration data and provide theoretical justification for their impact on learning efficiency. Next, we discuss how our multi-critic RL setup enables learning beyond the imitation dataset. Finally, to learn diverse skills in a single policy with inherent transitions, we incorporate modified versions of reference-state-initialization (RSI) and phase-based motion tracking without the original temporal dependence.

### 2.1 Decaying Action Priors

Sood et al. [20] proposed adding feedforward torques to the actions sampled by the policy during training, with the influence of these torques gradually decaying over time. The feedforward torques  $\beta_t$  are calculated as:  $\beta_t = K_p(\hat{\theta}_t - \theta_t) + K_d(-\dot{\theta}_t)$ . Where  $K_p$  and  $K_d$  are the PD parameters respectively,  $\hat{\theta}_t$  is the reference imitation angle while  $\theta_t$  and  $\dot{\theta}_t$  are the robot joint angles and velocities. These feedforward torques are added to the torque output  $\tau_t$  of the policy and the final output is sent to the robot as:  $\tau_t = a_t \sim \pi_\tau(s_t) + \gamma^{t/k}\beta_t$ , where  $a_t$  is the action sampled from the policy  $\pi_\tau$  at state  $s_t$ ,  $0 < \gamma < 1$  and  $k > 1$  are constants and  $t$  is the time-step. The feedforward torque  $\beta_t$  is added along with a term that reduces its influence over time and is referred to as an *action prior*. [20] demonstrated that leveraging action biases could accelerate learning for simple torque-based walking tasks, using perfect imitation data from a position-controlled policy. In contrast, we build on the core idea of action priors, and show how it can be synergistically integrated with recent advances in legged robot learning to propose a general imitation framework. We first formalize the role of action priors in structuring exploration and stabilizing policy optimization, providing theoretical and empirical evidence.

**Effect of Action Priors on PPO:** Adding action priors, as illustrated in Fig. 1, biases exploration toward physically plausible actions early in training. Combined with imitation rewards for these actions (Appendix), this keeps the policy exploring near a meaningful action space. This acts as a form of curriculum learning: initially, the agent experiences an easier MDP scaffolded by action priors, which gradually fade over time. We hypothesize that this scaffolding accelerates learning through two key mechanisms: (1) *Lower reward sparsity*: feedforward actions stabilize early behaviors, increasing reward density and speeding up initial learning; (2) *Stabilized PPO updates*: structured actions reduce the variance of advantage estimates, smoothing policy updates. Additionally, this structured exploration allows the policy to remain robust under heavy domain randomization

(DR) without collapsing to overly conservative behaviors, a common failure mode in many recent works [23, 11]. We validate these claims through extensive hardware experiments (3).

**Stabilized PPO Clipped Updates:** In Proximal Policy Optimization (PPO) [24], large and noisy policy updates are clipped using the surrogate objective:

$$L^{\text{PPO}}(\theta) = \mathbb{E}_t \left[ \min \left( r_t(\theta) \hat{A}_t, \text{clip}(r_t(\theta), 1 - \epsilon, 1 + \epsilon) \hat{A}_t \right) \right], \quad (1)$$

where  $r_t(\theta) = \frac{\pi_\theta(a_t|s_t)}{\pi_{\theta_{\text{old}}}(a_t|s_t)}$  is the probability ratio and  $\hat{A}_t$  is the advantage estimate. Early in training, random exploration can produce high-variance advantages  $\hat{A}_t$ , leading to unstable or frequently clipped updates. By introducing  $\beta_t$ , the actions  $a_t + \gamma^{t/k} \beta_t$  are more structured, reducing the variance in  $\hat{A}_t$ , and keeping  $r_t$  closer to 1. This reduces excessive clipping, leading to smoother and more efficient policy updates.

**Unbiasedness and Lower Variance of the APEX Blended-Action Policy Gradient** Although the environment experiences blended actions, the APEX policy gradient remains an unbiased estimator of the true objective gradient while benefiting from reduced variance. Specifically, even though the agent applies a blended action  $a_t^{\text{APEX}} = T(a_t, \beta_t, s_t)$ , where  $a_t \sim \pi_\theta(\cdot | s_t)$  and  $\beta_t$  is drawn from a fixed action prior, the performance objective

$$J(\theta) = \mathbb{E}_{\pi_{\text{APEX}}} \left[ \sum_{l=0}^{\infty} \gamma^l r_{t+l} \right]$$

has gradient  $\nabla_\theta J(\theta) = \mathbb{E} \left[ \nabla_\theta \log \pi_\theta(a_t | s_t) \hat{A}_t^{\text{APEX}} \right]$ , where  $\hat{A}_t^{\text{APEX}} = Q^{\pi_{\text{APEX}}}(s_t, a_t^{\text{APEX}}) - b(s_t)$  is an advantage estimator. The key insight here is that the blending operation  $T$  is deterministic and  $\theta$ -independent: it shapes exploration without altering the  $\theta$ -dependence of sampled actions. Thus, the standard REINFORCE derivation applies unchanged (more details in appendix).

## 2.2 Generalization to Tasks and Learning Diverse Behaviors

**Multi-Critic RL:** Balancing imitation and task exploration often demands tedious reward-weight tuning. The inter-dependence of these rewards will also hinder generalization to different terrains where it might either fit to the data more and not be able to explore or complete the task but not be able to replicate the imitation data’s style while doing so. To address these issues, we develop a *multi-critic* [25, 26, 27] setup. This ensures the policy can balance style imitation from flat-terrain data while generalizing to more challenging environments such as stairs and slopes. Specifically, we implement two critics: The **imitation critic**  $V_{\phi_{\text{imit}}}$  and the **task critic**  $V_{\phi_{\text{task}}}$ , each of which is updated independently based on their respective reward group. Training the two critics on disjoint reward groups provides the policy with distinct signals for “moving like the expert” and “solving the task,” helping balance the two objectives and significantly reducing the sensitivity to reward-weight tuning. We then integrate our multi-critic architecture into the PPO algorithm, where each critic is updated according to a standard temporal difference (TD) loss:

$$\mathcal{L}(\phi_i) = \mathbb{E}_t \left[ \left( r_t^i + \gamma \bar{V}_{\phi_i}(s_{t+1}) - V_{\phi_i}(s_t) \right)^2 \right], \quad i \in \{\text{imit}, \text{task}\}, \quad (2)$$

where  $\bar{V}_{\phi_i}$  is the corresponding target network.

**Learning Multiple Behaviors and Transitions:** Using our multi-critic with action priors, APEX learns individual skills effectively and generalizes them across a range of command velocities and environments. In order to enable smooth transitions between skills, despite such transitions being absent from the imitation data, and without relying on a separate high-level controller, we condition the policy on a normalized phase variable,  $\phi \in [0, 1]$ , inspired by prior work [21]. Unlike previous approaches, where phase tracks the progression through a full demonstration, we partition the phase space into intervals corresponding to different skills. During deployment, selecting and maintaining a constant phase executes a specific gait. This also enables the robot to switch to any gait at any time, without the need to sweep the phase variable from  $\phi = 0$  to  $\phi = 1$ , effectively removing

Table 1: Data Frame from Source and Usage Across Methods.

Input Type	Joint Angles	Toe Positions	Linear Velocity	Angular Velocity	Joint Velocity	Additional Keypoints*	Root Pos. (x,y)	Height (z)	Orientation
MoCap/Generated (Source)	–	Present	–	–	–	Present	Present	–	–
AMP (re-targeted)	Required	Required	Required	Required	Required	–	Required	Required	Required
APEX (re-targeted)	Required	Required	–	–	–	–	–	Optional	Optional

\*Spatial coordinates (x, y, z) of anatomical landmarks such as hips, knees, and neck, provided by the motion capture (MoCap) system for each frame.

the temporal dependence typically required to complete a full motion cycle. To further improve the learning efficiency, we rely on Reference State Initialization (RSI), initializing states based on randomly sampled phase values. However, unlike prior works, APEX only needs to reset joint angles using kinematic information during RSI, without the need for full dynamic state initialization.

### 3 Experimental Results

We evaluate and compare APEX with AMP [14], the current state-of-the-art framework for adversarial imitation learning. Additionally, we include comparisons with RL reward-based motion imitation approaches [21, 22] to highlight how APEX extends and improves upon this baseline.

We begin by comparing their performance in learning individual locomotion skills (gaits) through simulation benchmarks and real-world settings. Next, we demonstrate how our approach is able to unify multiple gaits within a single policy and validate its performance on hardware. We then showcase APEX’s ability to generalize beyond the original imitation data across various fronts. Finally, we highlight that APEX is not only easier to implement than AMP, but also more robust to DR and regularization.

**Imitation Data:** We primarily use a raw motion capture (MoCap) dataset [22], which consists of joint angles and foot positions over time. We first re-target this data to the Unitree Go2 using inverse kinematics on foot trajectories to produce joint angles consistent with the robot’s morphology. Further, we combined kinematic data from [8] with MoCap data to build a dataset of four gaits, demonstrating APEX’s ability to learn from heterogeneous data sources in a single unified policy. Unlike AMP, which relies heavily on joint velocities, root linear velocities, and angular velocities, which are highly sensitive to frame duration and sampling frequency specified in the motion loader, APEX depends only on simple, easily obtainable kinematic data (Table 1).

**Training Details and Comparisons:** All AMP and motion imitation policies were trained for 50k iterations, requiring approximately 18h to train on a 24 GB NVIDIA RTX4090 GPU. In contrast, APEX’s training runs 1k iterations, taking only 20min, highlighting its significantly improved sample efficiency and drastic reduction in training time. Full training configurations are provided in the appendix. Notably, AMP models trained for fewer iterations (e.g., 1k-50k) failed to reliably capture the intended style, often displaying unstable, oscillatory behavior, while further training beyond 50k showed no improvement. The baseline AMP configuration did not include regularization rewards and struggled with sim-to-sim transfer. To ensure a fair comparison, we enhanced AMP by incorporating regularization rewards and applying the same domain randomization strategy used in APEX. The best-performing AMP policies from this modified setup were used for evaluation.

#### 3.1 Single Skill Comparisons

**Simulation Evaluation:** We evaluate APEX, AMP, and motion imitation across four gaits—pace, prnk, trot, and canter by measuring RMS errors in velocity and height tracking against the corresponding commanded velocity and the single skill re-targeted imitation data. These evaluations are conducted in the training simulator (IsaacGym) and then tested under sim-to-sim transfer in MuJoCo. The results are summarized in Table 2. While agents trained with AMP tracked velocity and height reliably within the original training environment, their performance degrades significantly during sim-to-sim transfer, likely due to mode collapse—resulting in velocity errors as high as  $0.6m/s$ . Motion imitation not only fails to meet the task objective but also did not preserve the motion style. Its conservative behavior under domain randomization, combined with the absence of

Table 2: RMS errors in velocity and height tracking across different gaits in the training simulator (IsaacGym) and during sim-to-sim transfer (MuJoCo).

		Training Simulator				Sim-to-Sim			
		Pace 1m/s	Pronk 1m/s	Trot 1.5m/s	Canter 2m/s	Pace 1m/s	Pronk 1m/s	Trot 1.5m/s	Canter 2m/s
APEX	Vel. Error	<b>0.047</b>	0.087	0.088	<b>0.152</b>	<b>0.071</b>	<b>0.071</b>	<b>0.129</b>	<b>0.225</b>
	Height Error	<b>0.006</b>	0.038	0.014	0.031	0.093	<b>0.028</b>	<b>0.024</b>	0.045
AMP	Vel. Error	0.052	<b>0.052</b>	<b>0.0777</b>	0.192	0.284	0.434	0.452	0.624
	Height Error	0.037	<b>0.035</b>	<b>0.009</b>	<b>0.029</b>	<b>0.028</b>	0.039	0.037	0.071
Motion Imitation	Vel. Error	0.473	0.9999	1.500	2.000	0.467	0.9999	1.500	2.000
	Height Error	0.018	0.0435	0.053	0.049	0.092	0.044	0.034	<b>0.010</b>

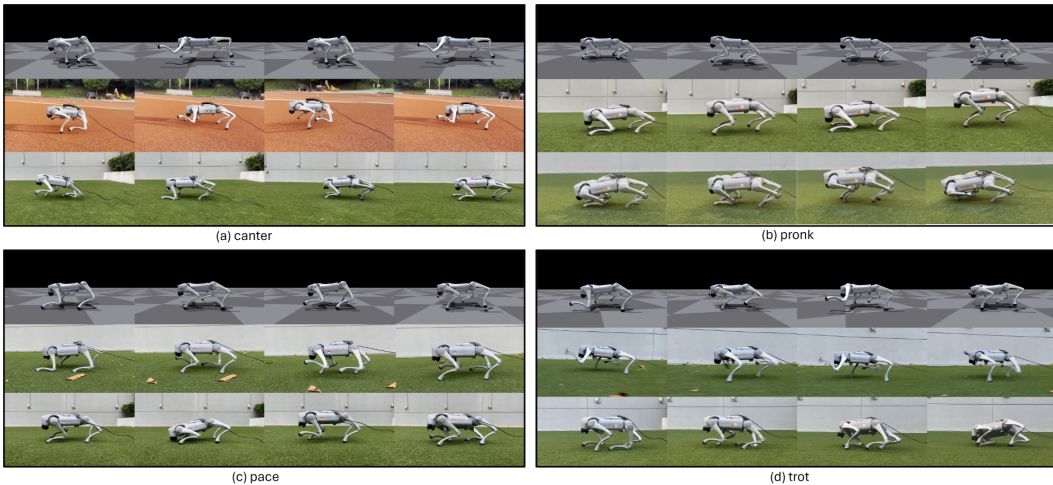


Figure 3: Comparison of single-gait execution in the real world. Each set of images shows the reference motion (top row), APEX (middle row), and AMP (bottom row). We note that APEX closely matches the reference style, while AMP exhibits noticeable deviations and instability.

action priors, leads it to overfit to height tracking, resulting in the low height tracking errors but high velocity tracking errors. In contrast, APEX consistently demonstrates stable performance across simulators. The agents maintain motion style and achieved consistently low velocity tracking errors as low as  $0.07m/s$  for pace.

**Preliminary Results on Humanoid:** In Fig.1 and the supplementary video, we show preliminary results of the Unitree-H1 humanoid learning to walk in simulation, using APEX, to highlight that our framework can generalize to other robot morphologies. We are currently working on extending APEX using recently released re-targeted human imitation datasets [28].

**Real World Evaluation:** APEX consistently outperformed AMP across all gaits in real-world zero-shot deployment. We first compare the single-gait AMP and APEX policies directly on hardware. Motion imitation policies were not deployed, as they exhibited high task tracking errors in simulation (see Table 2). On hardware, AMP-trained policies struggled across all single-gait experiments. As also reported by Huang et al. [17], AMP policies tended to oscillate around the reference motions with low amplitude and frequently failed, resulting in the robot falling. For instance, during execution of pace, the robot consistently fell after a few steps, while with pronk, it exhibited rapid vibrations and drifted in small circles before collapsing. These behaviors are illustrated in the appendix. In contrast, APEX-trained policies reliably reproduced the desired gaits on hardware without failure, as shown in (Fig. 3). They also successfully adapted to trained velocity ranges, maintaining stylistic consistency of the gaits even at high speeds. Remarkably, we achieved peak speeds  $> 3.3m/s$  on the robot while executing a three-beat canter gait. The velocity estimation details for this experiment can be found in the appendix.

### 3.2 Learning Diverse Skills in A Single Policy

APEX can learn multiple gaits in a single policy by adding our proposed normalized phase variable,  $\phi \in [0, 1]$ , to the agent’s observation. In our deployments, this phase can be mapped automatically

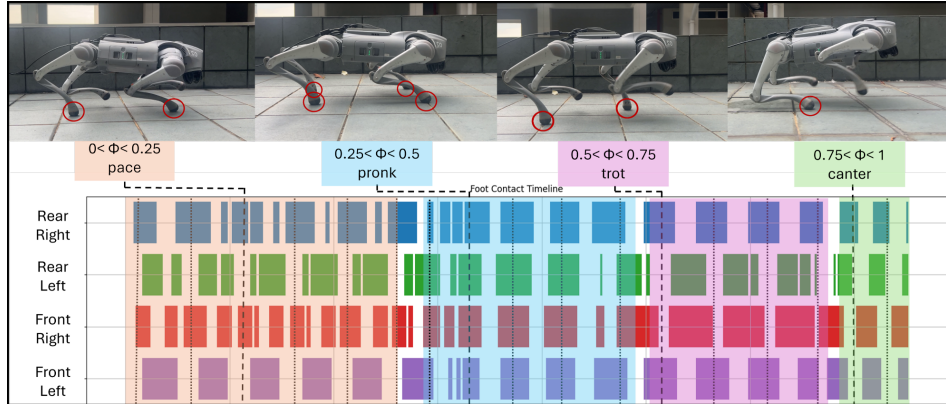


Figure 4: Gait pattern visualization of APEX multi-gait policy based on phase, with red circles indicating foot-ground contacts. The policy transitions through pace, pronk, trot, and canter, with the corresponding phase values.



Figure 5: (a) Canter gait on uneven slopes (b) Trot gait blindly walking on stairs 5/5 times (c) Robustness of policies trained on flat terrain on uneven terrain (pace gait shown).

to the commanded velocity or manually to a remote controller [8]. On hardware, APEX displayed distinct gait styles with clear footfall patterns across phase intervals (Fig. 4). The phase conditioning further allowed APEX to break free from strict velocity dependencies, enabling behaviors like a fast-paced canter at low speeds or direct transitions between gaits (e.g., canter to pace) without passing through intermediate gaits. In contrast, AMP-based multi-skill policies, despite relying on transition preloading and extensive motion sampling, failed to reliably generate all gaits even in simulation. For instance, a policy trained on pace, pronk, trot, and canter motions failed to produce canter, getting stuck instead in pronk or trot which are visualized in the appendix. While we attempted to improve this by integrating our phase-conditioning into AMP, it proved to be ineffective, as the random sampling of millions of preloaded transitions lacked temporal coherence, limiting the utility of the addition.

### 3.3 Generalization of Imitation Styles to Uneven Terrain

We finally tested APEX’s ability to generalize gaits to challenging terrains not present in the imitation data (Fig. 5). We train using only flat-ground imitation data with a rough-terrain curriculum like [29]. These policies are tested on hardware across three tasks: (1) executing canter up and down a  $\sim 30^\circ$  slope, (2) trotting over stairs (10, cm height) with a 5/5 success rate, and (3) performing pace on unstructured rough ground. When trained on rough terrain, APEX reliably completes all tasks using the intended gaits. In contrast, policies trained only on flat ground, while somewhat robust due to DR, struggle and often fail when deployed on real-world rough terrain. This demonstrates that APEX enables the robot to learn robust rough-terrain locomotion while preserving the stylistic qualities of the original imitation data. The results are best illustrated in the supplementary video. These experiments highlight that our exploration mechanism enables policies to generalize effectively from simple flat-ground data without deviating from the intended gait styles. In contrast, traditional supervised imitation approaches overfit to the imitation data and hence cannot generalize, while AMP suffers from mode collapse, leading to poor performance even on flat terrain.

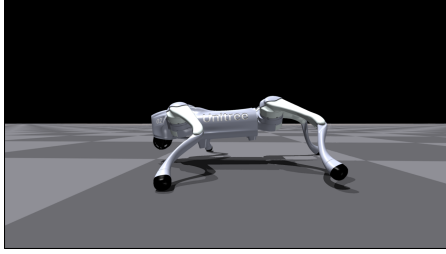


Figure 6: AMP learning erratic behavior without joint-velocity imitation data.

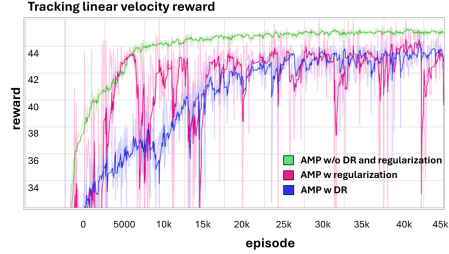


Figure 7: Reward returns of AMP with and without DR and regularization.

### 3.4 Additional Advantages of APEX

**No Need for Joint Velocities:** APEX is designed to operate using only kinematic data (joint angles and foot positions) without relying on joint velocities, which are often missing or unreliable in motion capture or video-derived datasets (Section 3). To evaluate whether AMP can similarly learn under these circumstances, we removed joint velocities from its input and performed extensive hyperparameter tuning. However, AMP consistently failed to learn meaningful behaviors and instead exhibited erratic motion (Fig.6), highlighting APEX’s superior suitability for real-world and low-fidelity data sources.

**Parameter Tuning:** APEX is robust to reward and parameter tuning, enabled by its scaffolded exploration and multi-critic architecture. We use fixed decay schedules for reward terms, with decay factors applied uniformly at 800 iterations out of 1k across all motions and tasks, without the need for motion-specific adjustments (see Appendix for details). In contrast, AMP required significant tuning to achieve stable performance in simulation. It was highly sensitive to the style reward coefficient (*amp\_reward\_coef*) and task blending factor (*task\_reward\_lerp*); improper settings led to degraded imitation quality or loss of stylistic fidelity.(details in appendix)

**Effect of DR and Regularization:** APEX demonstrates robust performance when trained with domain randomization (DR) and regularization. The reliance on kinematic action priors enables it to achieve tasks without becoming overly conservative under these effects. We evaluate the impact of DR and regularization on AMP training as shown in (Fig. 7). Incorporating DR (blue curves) and regularization (purple curves) results in more conservative policies, which exhibit excessive oscillations and less rewards. In contrast, APEX maintains the ability to learn both task objectives and stylistic features without becoming overly conservative, even when trained with DR and regularization, as shown in the training curves in the appendix.

## 4 Conclusion

We presented APEX, a simple yet effective imitation learning framework that combines reinforcement learning with action priors to enable efficient, diverse, and transferable legged locomotion. By biasing early exploration with decaying feedforward torques and decoupling imitation and task objectives via a multi-critic architecture, APEX achieves stable training, sample-efficient learning, and robust sim-to-real transfer. Unlike adversarial or diffusion-based approaches, APEX avoids common pitfalls such as mode collapse and high computational overhead, while still producing natural, agile, and diverse behaviors from kinematic demonstrations alone. Our results across a wide range of gaits, tasks, and hardware deployments, including stair climbing, terrain adaptation, and a peak hardware velocity of  $\sim 3.3$  m/s, demonstrate APEX’s strong generalization and real-world performance. We believe this work establishes APEX as a practical alternative to existing imitation learning methods and a promising direction for enabling more scalable and deployable robot learning systems.

## 5 Limitations and Future Work

While APEX demonstrates strong performance across diverse gaits and terrains, several limitations remain. First, certain learned gaits, such as canter, exhibit high foot-ground impact forces on hardware, suggesting that the current motion re-targeting process may not be fully optimized for the robot’s morphology. Improving the re-targeting process or fine-tuning the policies with additional energy-based rewards could enhance energy efficiency and reduce impact forces. Additionally, at the highest speeds, the canter gait policy struggles to accurately follow yaw commands, indicating potential limitations in stability and control at extreme velocities.

Second, during training, we occasionally observe drops in reward after the action priors decay. This suggests that the decay parameter ( $\gamma^{t/k}$ ) could be better integrated into the training process itself, rather than scheduled externally. Future work could involve adaptively adjusting this schedule based on policy performance to maintain stable learning.

Currently, the policy operates with limited sensory input, relying solely on single-timestep proprioceptive data without incorporating exteroceptive feedback. Integrating external sensors such as vision or depth could enable more responsive and terrain-aware behaviors, especially in complex or dynamic environments.

Finally, some of the limitations are rooted in the inherent characteristics of the imitation data itself. For example, the pace gait exhibits instability during stair climbing due to low foot clearance, while the canter gait, despite generalizing well to uneven terrain, suffers from knee impacts when ascending stairs—a result of its high-speed, low-clearance style. Expanding the dataset to include modified or augmented versions of such motions could help mitigate these style-induced limitations and improve overall robustness.

## References

- [1] R. Y. Siegwart, M. Hutter, P. Oettershagen, M. Burri, I. Gilitschenski, E. Galceran, and J. I. Nieto. Legged and flying robots for disaster response. 2015. URL <https://api.semanticscholar.org/CorpusID:113420886>.
- [2] J. Di Carlo, P. M. Wensing, B. Katz, G. Bledt, and S. Kim. Dynamic locomotion in the mit cheetah 3 through convex model-predictive control. In *2018 IEEE/RSJ International Conference on Intelligent Robots and Systems (IROS)*, pages 1–9, 2018. doi:10.1109/IROS.2018.8594448.
- [3] C. Dario Bellicoso, F. Jenelten, P. Fankhauser, C. Gehring, J. Hwangbo, and M. Hutter. Dynamic locomotion and whole-body control for quadrupedal robots. In *2017 IEEE/RSJ International Conference on Intelligent Robots and Systems (IROS)*, pages 3359–3365, 2017. doi:10.1109/IROS.2017.8206174.
- [4] C. Gehring, C. Dario Bellicoso, P. Fankhauser, S. Coros, and M. Hutter. Quadrupedal locomotion using trajectory optimization and hierarchical whole body control. In *2017 IEEE International Conference on Robotics and Automation (ICRA)*, pages 4788–4794, 2017. doi:10.1109/ICRA.2017.7989557.
- [5] D. Kim, J. Di Carlo, B. Katz, G. Bledt, and S. Kim. Highly dynamic quadruped locomotion via whole-body impulse control and model predictive control. *arXiv preprint arXiv:1909.06586*, 2019.
- [6] J. Hwangbo, J. Lee, A. Dosovitskiy, D. Bellicoso, V. Tsounis, V. Koltun, and M. Hutter. Learning agile and dynamic motor skills for legged robots. *Science Robotics*, 4, 2019. URL <https://api.semanticscholar.org/CorpusID:58031572>.
- [7] T. Miki, J. Lee, J. Hwangbo, L. Wellhausen, V. Koltun, and M. Hutter. Learning robust perceptive locomotion for quadrupedal robots in the wild. *Science robotics*, 7(62):eabk2822, 2022.

- [8] G. B. Margolis and P. Agrawal. Walk these ways: Tuning robot control for generalization with multiplicity of behavior. In *Conference on Robot Learning*, pages 22–31. PMLR, 2023.
- [9] A. Shirwatkar, V. K. Kurva, D. Vinoda, A. Singh, A. Sagi, H. Lodha, B. G. Goswami, S. Sood, K. Nehete, and S. Kolathaya. Force control for robust quadruped locomotion: A linear policy approach. In *2023 IEEE International Conference on Robotics and Automation (ICRA)*, pages 5113–5119, 2023. doi:10.1109/ICRA48891.2023.10161080.
- [10] T. He, C. Zhang, W. Xiao, G. He, C. Liu, and G. Shi. Agile but safe: Learning collision-free high-speed legged locomotion. *arXiv preprint arXiv:2401.17583*, 2024.
- [11] T. He, J. Gao, W. Xiao, Y. Zhang, Z. Wang, J. Wang, Z. Luo, G. He, N. Sobanbab, C. Pan, et al. Asap: Aligning simulation and real-world physics for learning agile humanoid whole-body skills. *arXiv preprint arXiv:2502.01143*, 2025.
- [12] F. Torabi, G. Warnell, and P. Stone. Behavioral cloning from observation. In *International Joint Conference on Artificial Intelligence*, 2018. URL <https://api.semanticscholar.org/CorpusID:23206414>.
- [13] J. Ho and S. Ermon. Generative adversarial imitation learning. In *Neural Information Processing Systems*, 2016. URL <https://api.semanticscholar.org/CorpusID:16153365>.
- [14] A. Escontrela, X. B. Peng, W. Yu, T. Zhang, A. Iscen, K. Goldberg, and P. Abbeel. Adversarial motion priors make good substitutes for complex reward functions. In *2022 IEEE/RSJ International Conference on Intelligent Robots and Systems (IROS)*, pages 25–32, 2022. doi:10.1109/IROS47612.2022.9981973.
- [15] R. Yang, Z. Chen, J. Ma, C. Zheng, Y. Chen, Q. Nguyen, and X. Wang. Generalized animal imitator: Agile locomotion with versatile motion prior. In *8th Annual Conference on Robot Learning*, 2024. URL <https://openreview.net/forum?id=9XV3dBqcf>.
- [16] J. Wu, G. Xin, C. Qi, and Y. Xue. Learning robust and agile legged locomotion using adversarial motion priors. *IEEE Robotics and Automation Letters*, 8(8):4975–4982, 2023. doi:10.1109/LRA.2023.3290509.
- [17] X. Huang, Y. Chi, R. Wang, Z. Li, X. B. Peng, S. Shao, B. Nikolic, and K. Sreenath. Dif-fuseloco: Real-time legged locomotion control with diffusion from offline datasets. In *8th Annual Conference on Robot Learning*, 2024. URL <https://openreview.net/forum?id=nVJm2RdPDu>.
- [18] R. Durall, A. Chatzimichailidis, P. Labus, and J. Keuper. Combating mode collapse in gan training: An empirical analysis using hessian eigenvalues. *arXiv preprint arXiv:2012.09673*, 2020.
- [19] J. Wu, Y. Xue, and C. Qi. Learning multiple gaits within latent space for quadruped robots. *ArXiv*, abs/2308.03014, 2023. URL <https://api.semanticscholar.org/CorpusID:260682916>.
- [20] S. Sood, G. Sun, P. Li, and G. Sartoretti. Decap : Decaying action priors for accelerated imitation learning of torque-based legged locomotion policies. *2024 IEEE/RSJ International Conference on Intelligent Robots and Systems (IROS)*, pages 2809–2815, 2023. URL <https://api.semanticscholar.org/CorpusID:263830010>.
- [21] X. B. Peng, P. Abbeel, S. Levine, and M. van de Panne. Deepmimic: Example-guided deep reinforcement learning of physics-based character skills. *ACM Trans. Graph.*, 37(4):143:1–143:14, July 2018. ISSN 0730-0301. doi:10.1145/3197517.3201311. URL <http://doi.acm.org/10.1145/3197517.3201311>.

- [22] X. B. Peng, E. Coumans, T. Zhang, T.-W. E. Lee, J. Tan, and S. Levine. Learning agile robotic locomotion skills by imitating animals. In *Robotics: Science and Systems*, 07 2020. doi:10.15607/RSS.2020.XVI.064.
- [23] T. He, Z. Luo, W. Xiao, C. Zhang, K. Kitani, C. Liu, and G. Shi. Learning human-to-humanoid real-time whole-body teleoperation. *2024 IEEE/RSJ International Conference on Intelligent Robots and Systems (IROS)*, pages 8944–8951, 2024. URL <https://api.semanticscholar.org/CorpusID:268264230>.
- [24] J. Schulman, F. Wolski, P. Dhariwal, A. Radford, and O. Klimov. Proximal policy optimization algorithms. *arXiv preprint arXiv:1707.06347*, 2017.
- [25] H. Liu, S. Teng, B. Liu, W. Zhang, and M. Ghaffari. Discrete-time hybrid automata learning: Legged locomotion meets skateboarding. *arXiv preprint arXiv:2503.01842*, 2025.
- [26] T. Huang, J. Ren, H. Wang, Z. Wang, Q. Ben, M. Wen, X. Chen, J. Li, and J. Pang. Learning humanoid standing-up control across diverse postures. *arXiv preprint arXiv:2502.08378*, 2025.
- [27] F. Zargarbashi, J. Cheng, D. Kang, R. Sumner, and S. Coros. Robotkeyframing: Learning locomotion with high-level objectives via mixture of dense and sparse rewards. *arXiv preprint arXiv:2407.11562*, 2024.
- [28] F. Al-Hafez, G. Zhao, J. Peters, and D. Tateo. Locomujoco: A comprehensive imitation learning benchmark for locomotion. In *6th Robot Learning Workshop, NeurIPS*, 2023.
- [29] N. Rudin, D. Hoeller, P. Reist, and M. Hutter. Learning to walk in minutes using massively parallel deep reinforcement learning, 2022. URL <https://arxiv.org/abs/2109.11978>.
- [30] E. Todorov, T. Erez, and Y. Tassa. Mujoco: A physics engine for model-based control. In *2012 IEEE/RSJ International Conference on Intelligent Robots and Systems*, pages 5026–5033. IEEE, 2012. doi:10.1109/IROS.2012.6386109.
- [31] W. Xu, Y. Cai, D. He, J. Lin, and F. Zhang. Fast-lid2: Fast direct lidar-inertial odometry. *IEEE Transactions on Robotics*, 38(4):2053–2073, 2022.
- [32] V. Makoviychuk, L. Wawrzyniak, Y. Guo, M. Lu, K. Storey, M. Macklin, D. Hoeller, N. Rudin, A. Allshire, A. Handa, and G. State. Isaac gym: High performance gpu-based physics simulation for robot learning, 2021.

## A Appendix

### A.1 Effect of Decaying Action Priors on PPO

**1. Unbiasedness of the APEX Blended-Action Policy Gradient** Let  $\pi_\theta(a | s)$  be a differentiable stochastic policy. Define the *APEX action* applied to the environment by

$$a_t^{\text{APEX}} = T(a_t, \beta_t, s_t) = a_t + \gamma^{t/k} \beta_t,$$

where  $a_t \sim \pi_\theta(\cdot | s_t)$ ,  $\beta_t$  is the action prior drawn from a fixed distribution  $p(\beta_t | s_t)$ , and  $T$  is a deterministic,  $\theta$ -independent blend with the action prior  $\beta_t$ . The environment therefore experiences the *blended policy*  $\pi_{\text{APEX}}$ . Its performance objective is

$$J(\theta) = \mathbb{E}_{\pi_{\text{APEX}}} \left[ \sum_{l=0}^{\infty} \gamma^l r_{t+l} \right]. \quad (3)$$

#### 1.1 Differentiate the Objective

$$\begin{aligned} \nabla_\theta J(\theta) &= \nabla_\theta \mathbb{E}_{s_t \sim d^{\pi_{\text{APEX}}}} \left[ \mathbb{E}_{a_t \sim \pi_\theta} \left[ Q^{\pi_{\text{APEX}}}(s_t, a_t^{\text{APEX}}) \right] \right] \\ &= \mathbb{E}_{s_t \sim d^{\pi_{\text{APEX}}}, a_t \sim \pi_\theta} \left[ \nabla_\theta \log \pi_\theta(a_t | s_t) Q^{\pi_{\text{APEX}}}(s_t, a_t^{\text{APEX}}) \right] \quad (\text{score-function identity}). \end{aligned} \quad (4)$$

**1.2 Insert a Baseline (critic)** Subtracting any baseline  $b(s_t)$  independent of  $a_t$  leaves the expectation unchanged:

$$\nabla_\theta J(\theta) = \mathbb{E} \left[ \underbrace{\nabla_\theta \log \pi_\theta(a_t | s_t)}_{\text{actor term}} \underbrace{\left( Q^{\pi_{\text{APEX}}}(s_t, a_t^{\text{APEX}}) - b(s_t) \right)}_{\hat{A}_t^{\text{APEX}}} \right]. \quad (5)$$

#### 1.3 Unbiased Gradient Estimator

Let

$$g_t = \nabla_\theta \log \pi_\theta(a_t | s_t) \hat{A}_t^{\text{APEX}}.$$

Since  $\mathbb{E}[g_t] = \nabla_\theta J(\theta)$ ,  $g_t$  is an *unbiased* estimator of the true policy gradient—even though the action executed in the environment is  $a_t^{\text{APEX}} = T(a_t, \beta_t, s_t)$ .

*Key intuition.* Every path from  $\theta$  to the return still passes through the random draw  $a_t$ . The deterministic blend  $T$  structures exploration (lowering the variance of  $\hat{A}_t^{\text{APEX}}$ ) but introduces no additional  $\theta$ -dependence, so the standard REINFORCE proof is unaffected.

**2. Stabilized PPO Clipped Updates:** In Proximal Policy Optimization (PPO) [24], the policy update is constrained to ensure stability by clipping large and noisy updates. This is achieved through the surrogate objective function:

$$L^{\text{PPO}}(\theta) = \mathbb{E}_t \left[ \min \left( r_t(\theta) \hat{A}_t, \text{clip}(r_t(\theta), 1 - \epsilon, 1 + \epsilon) \hat{A}_t \right) \right], \quad (6)$$

where  $r_t(\theta) = \frac{\pi_\theta(a_t | s_t)}{\pi_{\theta_{\text{old}}}(a_t | s_t)}$  is the probability ratio and  $\hat{A}_t$  is the advantage estimate.

The clipping operation restricts the policy update to a small neighborhood around the old policy, ensuring that changes are not too drastic. However, during the early stages of training, random exploration can lead to high variance in the advantage estimates  $\hat{A}_t$ . This can result in unstable policy updates or frequent clipping, which may slow down learning or prevent the policy from making meaningful progress. By introducing  $\beta_t$  (the expert feedforward actions), the actions  $a_t + \gamma^{t/k} \beta_t$  are more structured, reducing the variance in  $\hat{A}_t$ , and keeping  $r_t$  closer to 1. This reduces excessive clipping, leading to smoother and more efficient policy updates.

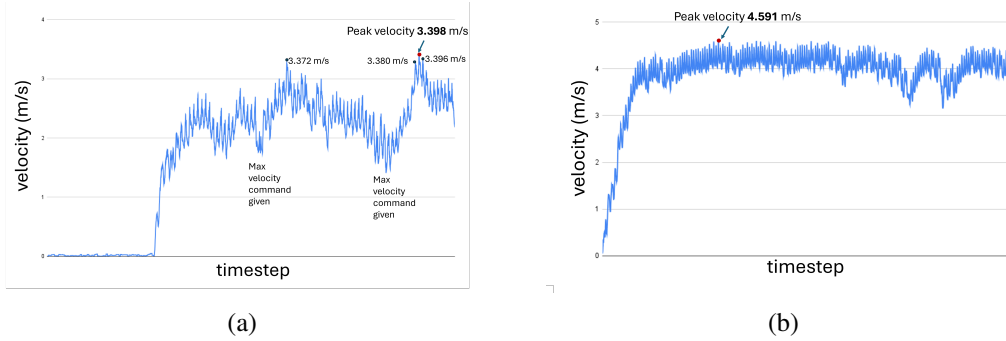


Figure 8: Velocity estimation graphs for (a) the real-world canter experiment, where peak velocities are marked corresponding to the given maximum velocity command. The peak velocity recorded in the real world was  $3.39m/s$ . (b) shows the velocity measured in sim-to-sim testing using MuJoCo [30].

## A.2 Velocity Estimation

We estimate the velocity of Go2 based on a state-of-the-art LiDAR-inertial odometry, Fastlio2 [31]. In particular, we use an iterated Kalman filter on the manifold (IKFoM) to estimate the velocity based on the propagation of IMU measurements. To eliminate the accumulated IMU measurements error, we refine the Kalman filter’s estimation when getting new Lidar measurements. By doing so, we get an accurate ( $< 0.03m/s$ ) and high-frequency ( $200Hz$ ) velocity estimation. We do not need the velocities as observations during hardware deployment. We only estimate the velocities to show the tracking in (Fig.8).

## A.3 AMP Parameter Tuning

In the AMP framework, the final reward  $r$  given to the policy is a linear interpolation between a discriminator-based style reward  $r_{style}$  and a task reward  $r_{task}$ :

$$r = (1 - \lambda_{task}) r_{style} + \lambda_{task} r_{task}$$

where  $\lambda_{task} \in [0, 1]$  controls the trade-off between style imitation and task accomplishment. The style reward is computed as:

$$r_{style} = \alpha \max \left( 1 - \frac{(d-1)^2}{4}, 0 \right)$$

where  $\alpha$  is the style reward coefficient (`amp_reward_coef`) and  $d$  is the discriminator output, ideally close to 1 for expert-like style. We observed that reducing  $\alpha$  from 2(default) to 1 significantly degraded learning, with policies failing to capture any of the distinct gait styles (pace, trot, and canter) even after 50k iterations. Similarly, increasing  $\lambda_{task}$  from 0.3(default) to 0.5 shifted optimization towards task completion at the expense of stylistic fidelity. Even when using the provided default parameters, the policy struggled to consistently reproduce complex motions like canter in a multi-gait training setup, particularly over command velocities in  $[0, 2]m/s$ . This indicates a high sensitivity of the learning outcome to discriminator reward scaling. Proper tuning of  $\alpha$  and  $\lambda_{task}$  is therefore critical for achieving robust imitation across diverse locomotion behaviors.

## A.4 APEX and AMP Comparisons:

**AMP Sim-to-Sim Results:** When policies trained in IsaacGym [32] were tested in MuJoCo [30], they struggled to reproduce reliable gaits. As seen in the (Fig. 9a), the robot limbs tend to oscillate around the desired motions with less amplitude and high frequency leading to failures. Pace experiences multiple body fluctuations and pronk revolves unstably in circles.

**Multiple Skills in AMP:** When trained on all motions available using AMP, (Fig. 10) shows the emergence of gaits in policies trained in IsaacGym [32], where the robot successfully learns several



Figure 9: AMP-generated gaits in MuJoCo: (a) pace and (b) pronk.

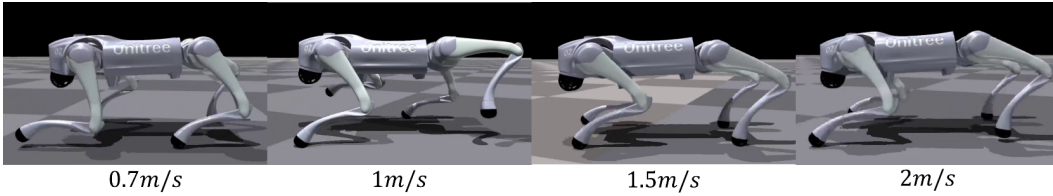


Figure 10: AMP gait progression in simulation when trained on pace, pronk, trot, and canter (left to right) over 50k iterations. The canter gait failed to emerge; instead, the policy learned to pronk at the given speed.

skills but fails to learn to canter. (Fig. 11) presents a real-world comparison of the multi-skill policies trained with APEX and AMP.

#### A.5 Effect of Different APEX Parameters

We analyze how varying the key parameters of the decaying action priors influences the mean training reward. As shown in (Fig. 12), the training process is relatively robust to changes in the parameter  $k$ , which was varied from 60 to 110 in increments of 10. In contrast, the parameter  $\gamma$  plays a more critical role. Higher values of  $\gamma$  are crucial for strongly biasing the policy toward imitation behaviors early in training, which significantly impacts performance.

#### A.6 Effect of Multi-Critic

Employing a multi-critic architecture allows the policy to optimize multiple objectives independently, reducing interference between them. This approach has proven effective in the legged robotics community [27, 25, 26]. As shown in (Fig.13), when training a trot gait on uneven terrain within the APEX framework, switching from a multi-critic to a single-critic setup, while keeping all other components constant, results in a policy that can learn the velocity tracking task but fails to generalize well to the imitation objective (shown by the (a) end-effector position tracking and, (b) imitation angle rewards). This highlights the advantage of decoupled optimization via separate critics, in line with prior findings in the field.

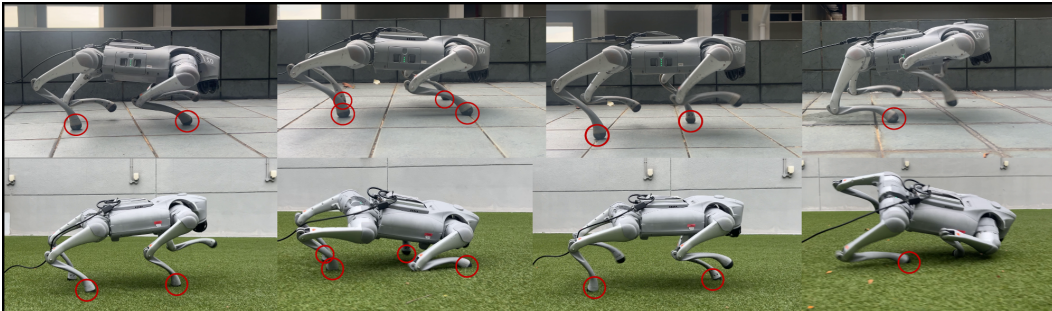
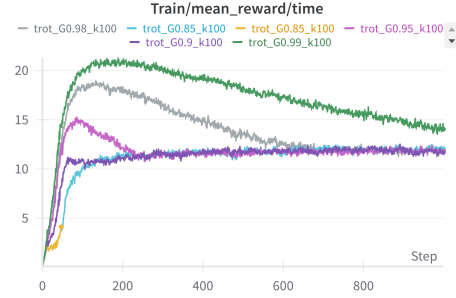


Figure 11: Multi-skill policy comparison in our real world experiments, showing APEX (top) (trained for 1k iterations), and AMP (bottom) (trained for 50k iterations) for pace, pronk, trot, and canter from left to right.

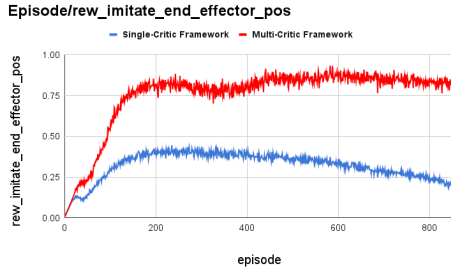


(a) Varying  $k$

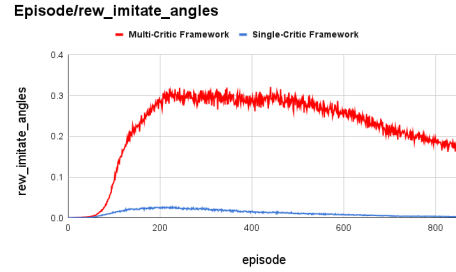


(b) Varying  $\gamma$

Figure 12: Mean reward comparison while training a trot gait with different APEX parameters  $k$  and  $\gamma$  show that actions priors are robust to changes in  $k$  but can vary with huge changes to the  $\gamma$  term.



(a)



(b)

Figure 13: Comparison of reward trends for (a) end-effector position and (b) imitation angles tracking.

### A.7 Generalization to Different Linear and Angular Velocities

All imitation data was collected at a fixed linear velocity specific to each gait: 0.4 m/s for pronk, 1 m/s for pace, 1.5 m/s for trot, and 2 m/s for canter. Despite this limited training distribution, APEX generalizes effectively across a wide range of commands—covering linear velocities from 0 to 2 m/s and angular velocities from  $-1.5$  to  $1.5$  rad/s for all gaits. Notably, for canter, APEX generalizes up to 4.5 m/s in sim-to-sim settings. Velocity tracking performance is illustrated in (Fig. 14).

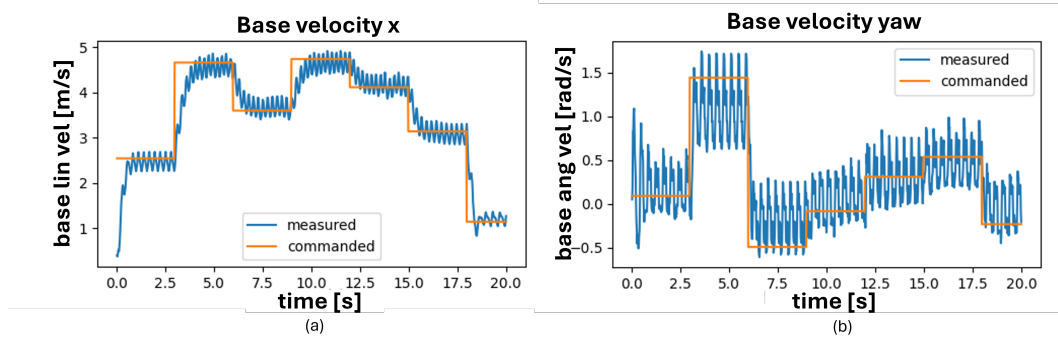


Figure 14: Velocity tracking performance: (a) linear velocity, (b) angular velocity.

### A.8 Normalized Reward Graphs of Imitation Alone Vs APEX with Imitation

Another common and simpler method of motion imitation is just using the imitation data as rewards [22] for the policy along with reference state initialization and phase based tracking [11]. We also compare this method against APEX. In our implementation, imitation rewards are preserved and the multi-critic architecture remains unchanged. However, we observed that under heavy domain randomization (DR), policies trained using this baseline tend to adopt overly conservative behaviors 15. In contrast, APEX’s scaffolding mechanism enables more effective utilization of imitation data in the same conditions. We hypothesize that this is because the action priors in APEX encourage the emergence of imitation behaviors early in training—even under heavy DR—while also supporting the policy with more stable guidance. This reduces the likelihood of catastrophic failures, allowing the policy to remain in higher-reward regions and reinforcing the imitation behaviors through repeated success.

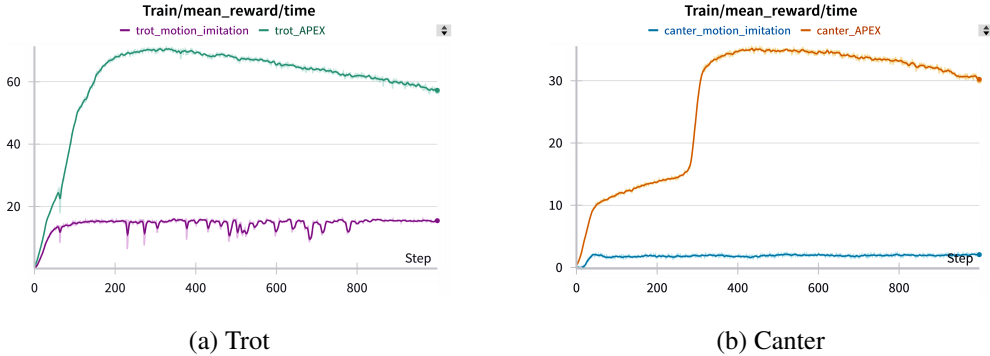


Figure 15: Mean reward comparison across gaits to compare the impact of domain randomization and regularization rewards on policies trained using motion imitation vs APEX.

### A.9 Training setup, Observation and Action Space:

We utilize IsaacGym [32] as the training environment and MuJoCo [30] as the sim-to-sim testing environment. The task is to track given linear and angular velocity commands while imitating the gaits from the animal motion capture (MoCap) data. For the observations we use proprioceptive data from onboard sensors, including the IMU and joint encoders. The observation space is defined as  $\mathcal{O}_{\square} = [g_{\text{proj}}, v_t^{\text{cmd}}, \omega_t^{\text{cmd}}, q_t, \dot{q}_t, a_{t-1}]$  where  $g_{\text{proj}}$  is the gravity vector projected into the robot’s base frame,  $v_t^{\text{cmd}}$  and  $\omega_t^{\text{cmd}}$  are the user-provided linear (x, y) and angular velocity commands, respectively,  $q_t$  and  $\dot{q}_t$  are the joint positions and velocities, and  $a_{t-1}$  is the previous unscaled action output by the policy. The action space is a vector with the same dimension as the number of actuators scaled by a constant factor (0.25 in our case). These actions are then sent to the robot as positions commands by converting them to torques using a Proportional Derivative (PD) controller. We set  $k_p = 20$  and  $k_d = 0.5$ . During training, we use an asymmetric actor-critic setup, where the critic receives privileged information—including the true linear and angular velocities, and the terrain height map (in the case of uneven terrain)—while the actor’s observations remain unchanged and limited to onboard sensors. Additional training details are provided in Table 3.

### A.10 Reward Terms

The reward terms, their expressions, weights, and corresponding groups are listed in Table 4.

### A.11 Domain Randomization:

We randomize the parameters listed in Table 5 within specified ranges to ensure effective sim-to-real transfer of the trained policies for both APEX and AMP.

Hyperparameter	Value
Max Policy Iterations	1000
Steps per Environment per Iteration	24
Number of Environments	4096
Observation Dimension	42*
Privileged Observation Dimension	48*
Number of Critics	2
Entropy Coefficient	0.01
Discount Factor ( $\gamma$ )	0.99
GAE Lambda ( $\lambda$ )	0.95
Learning Rate	$1 \times 10^{-3}$
Value Loss Coefficient	1.0
PPO Clip Parameter	0.2
Mini-batches per Iteration	4
Epochs per Iteration	5
Optimizer	Adam

Table 3: RL training hyper-parameters (trained on a single RTX 4090 GPU).

\*for the multi-skill policy, we also include the phase variable in the observation space.

Reward Term	Expression	Weight
<i>Task Rewards (Group 1a)</i>		
Linear velocity tracking	$\phi \left( \mathbf{v}_t^{\text{cmd}} - \mathbf{v}_t \right)$	1.0
Angular velocity tracking	$\phi \left( \boldsymbol{\omega}_t^{\text{cmd}} - \boldsymbol{\omega}_t \right)$	0.9
<i>Regularization Rewards (Group 1b)</i>		
Feet air-time	$\left( \sum_{i=1}^{n_{\text{feet}}} (t_{\text{air}, i} - 0.5) \cdot \mathbf{1}_{\text{first contact}, i} \right) \cdot \mathbf{1}_{\ \mathbf{v}_t^{\text{cmd}}\  > 0.1}$	1.0
Feet slip	$\ \mathbf{v}_{xy}^{\text{foot}}\ $	-0.04
Torques	$-\ \boldsymbol{\tau}\ ^2$	-0.0001
Action rate	$-\ \dot{\mathbf{q}}_t^*\ ^2$	-0.01
Body height penalty	$(h_z - h_z^{\text{cmd}})^2$	-30.0
<i>Multi-Critic Rewards (Group 2)</i>		
Imitation: joint angles	$\ \boldsymbol{\phi}_t - \boldsymbol{\phi}_t^{\text{ref}}\ ^2$	1.5
Imitation: end-effector position	$\ \mathbf{p}_{xy}^{\text{foot}} - \mathbf{p}_{xy}^{\text{ref}}\ ^2$	1.5

Table 4: Reward structure: task rewards, regularization rewards, and multi-critic imitation rewards.

Parameter	Range / Value
Added Mass for the base	[-1.0, 2.0]
Friction	[0.3, 1.25]
Push interval (s)	5
Max push velocity (xy)	2.0
Max push velocity (angular)	1.5
Motor offset range	[-0.03, 0.03]
Motor strength ratio	[0.8, 1.2]
COM shift (x)	[-0.2, 0.2]
COM shift (y)	[-0.1, 0.1]
COM shift (z)	[-0.1, 0.1]

Table 5: Domain Randomization Parameters.

## A.12 APEX with Multi Critic

The pseudo-code for the implementation of multi-critic PPO algorithm with decaying action priors is shown in 1:

---

### Algorithm 1: Multi-Critic Single-Actor PPO w/ Decaying Action Priors

---

**Input:** Policy  $\pi_\theta$ , critics  $V_{\phi_{\text{task}}}, V_{\phi_{\text{imit}}}$ ,  
 decay params  $(\gamma, k)$ , PPO clip  $\epsilon$ ,  
 rollout length  $T$ , epochs  $K$ , learning rates  $\alpha_\pi, \alpha_c$

**for each iteration do**

```

// --- Collect Rollout ---
for  $t = 0$  to  $T - 1$  do
   $a_t \sim \pi_\theta(\cdot | s_t)$ ;
   $a_t^{\text{APEX}} \leftarrow a_t + \gamma^{t/k} \beta_t$  where  $\beta_t = K_p(\hat{\theta}_t - \theta_t) + K_d(-\dot{\theta}_t)$ ;
   $(s_{t+1}, r_t^{\text{task}}) \leftarrow \text{Env}(s_t, \tau_t)$ ;
   $r_t^{\text{imit}} \leftarrow$  (imitation reward);
  store  $(s_t, a_t, r_t^{\text{task}}, r_t^{\text{imit}}, s_{t+1})$ 
// --- Compute Advantages via GAE ---
Compute  $\hat{A}_{\text{task}}$  w.r.t.  $r^{\text{task}}$  and  $V_{\phi_{\text{task}}}$ ;
Compute  $\hat{A}_{\text{imit}}$  w.r.t.  $r^{\text{imit}}$  and  $V_{\phi_{\text{imit}}}$ ;
 $\hat{A}_{\text{MuC}} = \sum_{i=0}^n w_i \frac{\hat{A}_i - \mu_{\hat{A}_i}}{\sigma_{\hat{A}_i}}$ ;
// --- PPO Updates ---
for  $\text{epoch} = 1$  to  $K$  do
  Update critics;
  Compute  $r_t(\theta) = \frac{\pi_\theta(a_t | s_t)}{\pi_{\theta_{\text{old}}}(a_t | s_t)}$ ;
   $L_t(\theta) = \min(r_t(\theta) \hat{A}_{\text{MuC}}, \text{clip}(r_t(\theta), 1 - \epsilon, 1 + \epsilon) \hat{A}_{\text{MuC}})$ ;
   $\theta \leftarrow \theta + \alpha_\pi \nabla_\theta \frac{1}{T} \sum_t L_t(\theta)$ 
 $\theta_{\text{old}} \leftarrow \theta$ 

```

---